Supplementary Information (SI) for Energy & Environmental Science.
This journal is © The Royal Society of Chemistry 2024

Supplementary Information (SI)

Unveiling nanoscale fluid miscible behaviors with nanofluidic slim-tube

Zengding Wang [a], Tianjiang Zhang [a], Shanchao Liu [a], Keli Ding [a], Tengyu Liu [a], Jun Yao [a], Hai Sun [a], Yongfei Yang [a], Lei Zhang [a], Wendong Wang [a], Cunqi Jia [b], Mojdeh Delshad [b], Kamy Sepehrnoori [b], Junjie Zhong [a]*

[a] *State Key Laboratory of Deep Oil and Gas, China university of Petroleum (East China), Qingdao 266580, P.R. China*
[b] *Hildebrand Department of Petroleum and Geosystems Engineering, The University of Texas at Austin, Austin TX78712, USA*

*Corresponding authors. Email address: zhongjunjie@upc.edu.cn (J.Z.)

TABLE OF CONTENTS

Section 1: Displacement pressure drop applied in experiment

To determine the suitable displacement pressure drop, we evaluated the threshold pressure corresponding to the lowest CO_2 injection pressure in each set of MMP measurements. This threshold pressure is used as the displacement pressure drop of the MMP experiment to avoid the influence of flow on the MMP measurement. For instance, we conducted a CO_2 flooding heptane with injection pressure ranging from 5.4 to 6.2 MPa using an irregular model at 25 ℃. The capillary force measured was 0.1 MPa when CO_2 injection pressure is 5.4 MPa. Consequently, the displacement pressure drop utilized in this group MMP experiment within the 5.4~6.2 MPa injection pressure range is 0.1 MPa. Given that the capillary force varies with injection pressure, chip model, temperature, and fluid composition, the displacement pressure employed in our experiments may vary, albeit consistently within the same set of miscible pressure measurement experiments. Across all our experimental endeavors, the displacement pressure drop typically ranges from 0.1 to 0.2 MPa. Table S1-S3 showed the displacement pressure drop used in MMP measurements within different physical models.

Table S1 Displacement pressure drops used in regular nanopore model.

	Temperature (℃)		
	25	35	45
Fluid component	Pressure drop (MPa)		
CO_2-heptane	0.1	0.1	0.1
CO_2-pentane-dodecane	0.2	N/A	0.2

Table S2 Displacement pressure drops used in irregular nanopore model.

	Temperature (℃)			
	25	35	45	55-130
Fluid component	Pressure drop (MPa)			
CO_2-heptane	0.1	0.1	0.1	0.2
CO_2-pentane-dodecane	0.2	N/A	0.2	N/A

Table S3 Displacement pressure drops used in multiscale model.

	Temperature (°C)	
	25	45
Fluid component	Pressure drop (MPa)	
CO_2-heptane	0.2	0.2
CO_2-pentane-dodecane	0.2	0.2

Section 2: Effect of displacement time on displacement ratio

Regarding displacement time, we injected CO_2 until the hydrocarbon phase area in the whole porous medium no longer changed. Fig. S1 showed the cumulative displacement ratio of heptane changes with time in irregular nanopore model at 25 °C and 5.6 MPa (below MMP). The findings indicate an initial surge in the cumulative displacement ratio of heptane, succeeded by a phase of stabilization. Subsequently, as the CO_2 front breaks through the observation area (220 s), the cumulative displacement ratio of heptane persists in its ascent until the displacement ratio stabilizes at 69.33%, achieved after a displacement time exceeding 460 s.

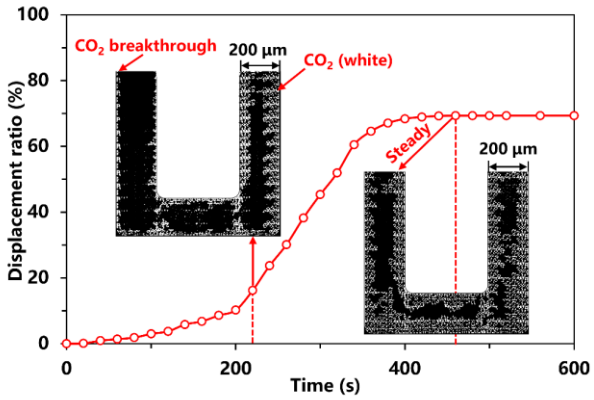

Fig. S1 Cumulative displacement ratio of heptane changing with time in irregular nanopore model at 25 °C and 5.6 MPa.

Similarly, Fig. S2 illustrated the cumulative displacement ratio of heptane changes with time in the irregular nanopore model at 25 °C and 6.2 MPa (MMP). The result showed that the cumulative displacement ratio of heptane stabilized at 100% when the displacement time exceed 42 s. Consequently, irrespective of CO_2 injection pressure, displacement ratio of hydrocarbon remains constant regardless of displacement time once flow stabilization occurred. In our experiment, the displacement ratio is calculated based on captured images after displacement stabilization.

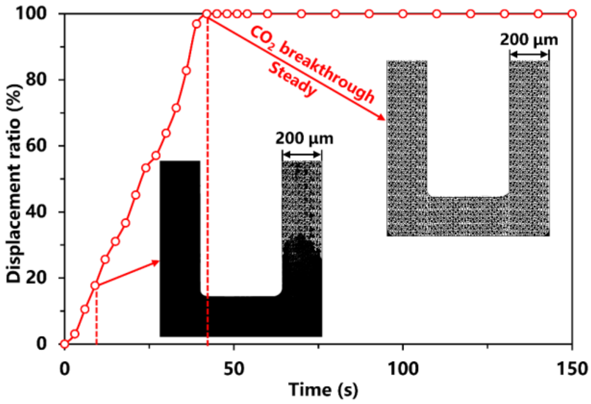

Fig. S2 Cumulative displacement ratio of heptane changing with time in irregular nanopore model at 25 °C and 6.2 MPa.

Section 3: Comparison of convection and diffusion rates

We recorded the process of CO_2 immiscible displacement of the pentane/dodecane mixture in the regular nanopore model at 25 °C and 5.2 MPa to compare the rates of convection and diffusion. Two sets of points were selected: group A (A1, A2) and group B (B1, B2) along the axial section of the porous media (Fig. S3a). The line connecting points A1 and A2 is vertical, with a distance of 300 μm. Similarly, the line connecting points B1 and B2 is also vertical and measures 300 μm. We documented the changes in the gray values of these two set of points during immiscible displacement (Fig. S3b and S3c). The gray value is used as a qualitative indicator for fluid composition changes.

The variation patterns of the gray values for both sets of points are similar. In the initial stage, both points A1 and A2 have gray values of 70 ± 4, indicating negligible CO_2 dissolution in the pentane/dodecane mixture. As the CO_2 diffusion front enters the observation area, CO_2 molecules diffuse and largely dissolve in the pentane/dodecane mixture, resulting in a sharp increase in the gray value of the pentane/dodecane phase (130 ± 10). The diffusion front reaches point A1 at 208 s and point A2 at 210 s, yielding a diffusion velocity of approximately 150 μm/s. Similarly, the CO_2 displacement front fully displaces the pentane/dodecane mixture (with gray values of 170) at 232 s for A1 and 262 s for A2, result in convection velocity of 10 μm/s. Analyzing group B confirmed these trends, with the same diffusion velocity (150 μm/s) and convection velocity (10.7 μm/s) observed. These results demonstrate that CO_2 diffusion velocity significantly surpasses convection velocity in nanopores, confirming the dominant role of diffusion in mass transport within nanoporous media.

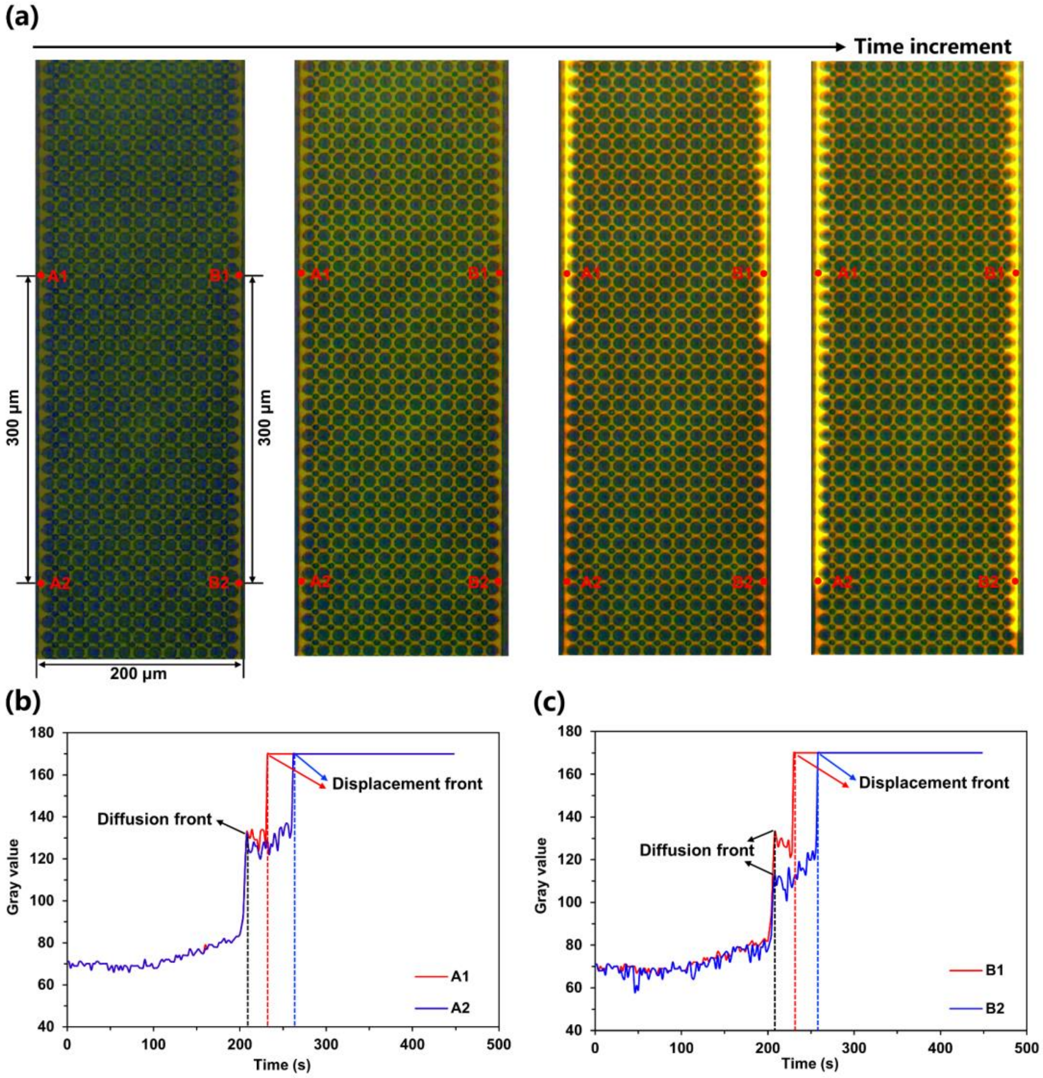

Fig. S3 Visualization of CO_2 immiscible displacement in the regular nanopore model. (a) Images captured at different stages of mass transport for CO_2 and pentane/dodecane in the nanoporous medium at 25 °C and 5.2 MPa. (b) Time-dependent variation in gray value of fluid at two fixed positions, A1 and A2, marked in (a). (c) Time-dependent variation in gray value of fluid at two fixed positions, B1 and B2, marked in (a).

Section 4: Video of CO_2 immiscible and miscible displacement in irregular nanopore model

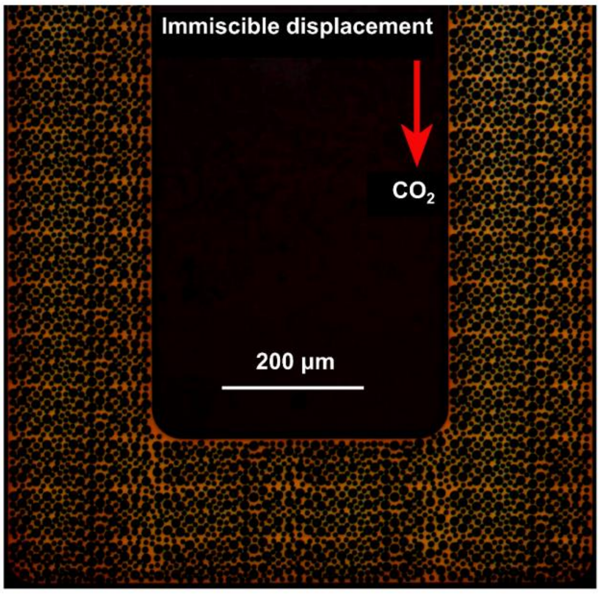

Fig. S4 CO_2 immiscible displaces pentane-dodecane in irregular nanopore model at 25 °C and 5 MPa (6.6x speed).

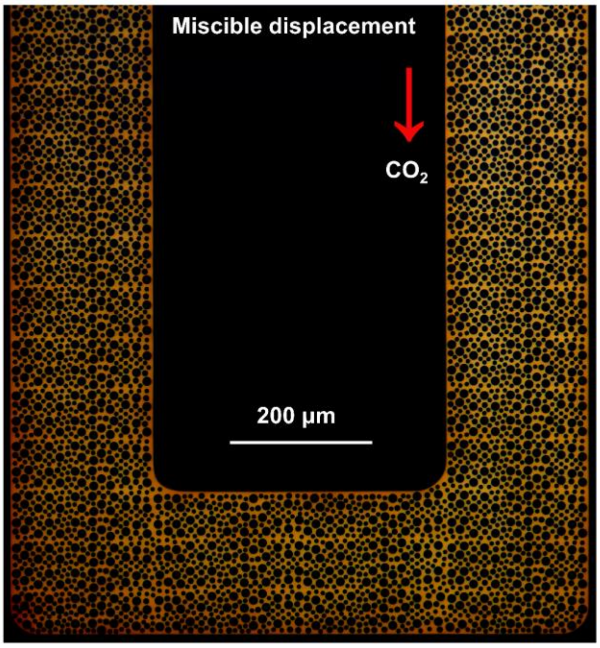

Fig. S5 CO_2 miscible displaces pentane-dodecane in irregular nanopore model at 25 °C and 6.2 MPa (2x speed).

Section 5: Video of CO_2 immiscible and miscible displacement in multiscale model

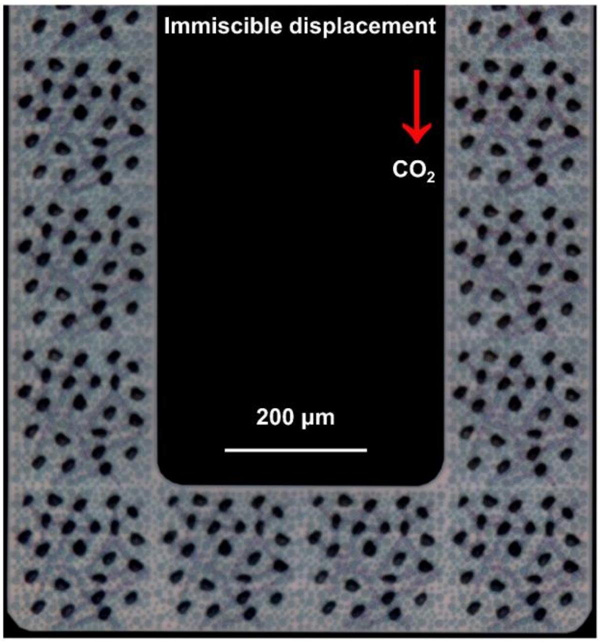

Fig. S6 CO_2 immiscible displaces pentane-dodecane in multiscale model at 45 °C and 7.4 MPa (60x speed).

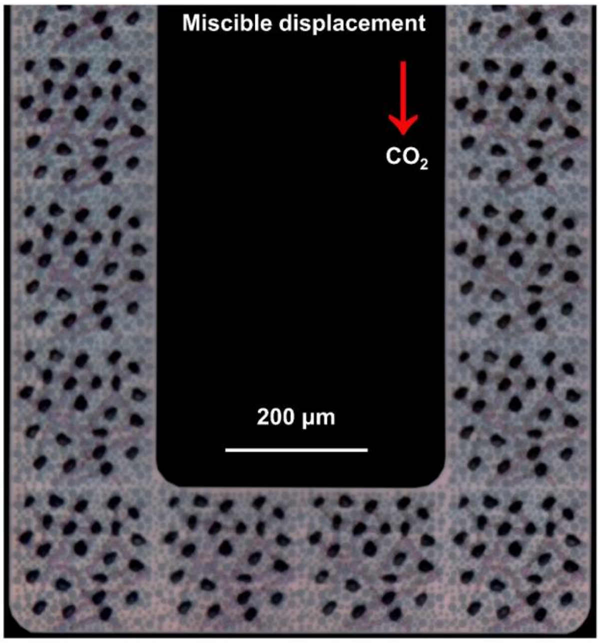

Fig. S7 CO_2 miscible displaces pentane-dodecane in multiscale model at 45 °C and 9.6 MPa (10x speed).

Section 6: Method for calculating nanoscale MMP based on modified PR-EOS

6.1 Modified PR-EOS with adsorption effect

In this work, we used the modified PR-EOR with selective adsorption effect for phase behavior calculation to consider the non-uniform density distribution of fluid molecules in nanopores.[S1] The expression of the modified PR-EOS is as follows:

$$P=\frac{RT}{\frac{V_m}{1-\chi}-b}-\frac{a\alpha(T)}{\frac{V_m}{1-\chi}(\frac{V_m}{1-\chi}+b)+b(\frac{V_m}{1-\chi}-b)} \tag{S1}$$

$$a=0.45724\frac{R^2T_c^{\ 2}}{P_c} \tag{S2a}$$

$$b=0.0778\frac{RT_c}{P_c}(1-\chi) \tag{S2b}$$

$$\chi=0.8594\times(\frac{r_e}{\sigma_{LJ}})^{-1} \tag{S2c}$$

$$r_e=r_p-\delta \tag{S2d}$$

where P is the system pressure, T is the system temperature, V_m is the molar volume of fluid, a is the attraction parameter in PR-EOS, b is the volume parameter in PR-EOS, $\alpha(T)$ is the alpha function, R is the universal gas constant, χ is the adsorption ratio, r_p is the original pore radius, δ is the adsorption layer thickness, r_e is the effective pore radius, σ_{LJ} is the Lennard-Jones size parameter.

An empirical method is used to estimate adsorption layer thickness in Eq. (S2d).[S2]

$$\delta=o(r_p)^p+q \tag{S3}$$

$$o=-8.789MW^{-1.316}+0.5018 \tag{S4a}$$

$$p=1.079\times10^{-4}MW^{1.322}-0.6188 \tag{S4b}$$

$$q=-0.7506\times MW^{-0.2881}+0.38 \tag{S4c}$$

where o, p and q are fitting parameters.

6.2 Critical point shift

The critical point shift of confined fluid is related to the dimensionless pore radius, which is defined as the ratio of pore radius (r_e) to the Lennard-Jones size parameter (σ_{LJ}). Using the collect data from previous experiments and molecular simulations, the empirical correlation between critical temperature shift (ΔT_c) and the dimensionless pore radius, as well as the correlation between critical pressure shift (ΔP_c) and the dimensionless pore radius are developed:

$$\Delta T_c = 0.8594 \times (\frac{r_e}{\sigma_{LJ}})^{-1} \tag{S5a}$$

$$\Delta P_c = 1.7188 \times (\frac{r_e}{\sigma_{LJ}})^{-1} - 0.7386 \times (\frac{r_e}{\sigma_{LJ}})^{-2} \tag{S5b}$$

6.3 Capillary force effect

Capillarity causes an additional pressure difference between vapor and liquid. We assumed that the liquid and vapor are wetting phase and non-wetting phase, respectively. Thus, the correlation between capillary pressure (P_{cap}), vapor phase pressure and liquid pressure phase can be expressed as:

$$P_{cap} = P_V - P_L \tag{S6}$$

The Young-Laplace equation is used to calculate capillary pressure in nanopores.

$$P_{cap} = \frac{2\sigma \cos\theta}{r_e} \tag{S7}$$

where σ is the interfacial tension, θ is the contact angle. Here the contact angle equals 0 as the nanopore surface is assumed to be completely liquid-wetting.

The Parachor model is used to predict the IFT of the liquid-vapor system.

$$\sigma = [p(\rho_L - \rho_V)]^4 \tag{S8a}$$

where p is the parachor number, ρ_L is the liquid density, ρ_V is the vapor density. For a multicomponent system, Eq. (S8a) is extended to Macleod-Sugden equation:[S3]

$$\sigma = (\rho_L \sum_{i=1}^{N_c} x_i p_i - \rho_V \sum_{i=1}^{N_c} y_i p_i)^4 \tag{S8b}$$

where x_i and y_i are the molar percentages of component i in the liquid and vapor phases, respectively. Since $\rho_L = \frac{P_L MW_L}{Z_L RT}$, $\rho_V = \frac{P_V MW_V}{Z_V RT}$, Eq. (S8b) can be rewritten as:

$$\sigma = (\frac{P_L MW_L}{Z_L RT}\sum_{i=1}^{N_c} x_i p_i - \frac{P_V MW_V}{Z_V RT}\sum_{i=1}^{N_c} y_i p_i)^4 \tag{S8c}$$

where MW_L is the molar weight of the liquid phase, MW_V is the molar weight of the vapor phase.

6.4 Nanoscale CO_2-hydrocarbon MMP calculation

The compressibility of liquid or vapor phase is determined by the modified PR-EOS as:

$$Z_L^3 - (1-B_L)Z_L^2 + (A_L - 3B_L^2 - 2B_L)Z_L - (A_L B_L - B_L^2 - B_L^3) = 0 \tag{S9a}$$

$$Z_V^3 - (1-B_V)Z_V^2 + (A_V - 3B_V^2 - 2B_V)Z_V - (A_V B_V - B_V^2 - B_V^3) = 0 \tag{S9b}$$

where:

$$A_L = \frac{a\alpha(T)P_L}{(RT)^2} = 0.45724\alpha(T)\frac{P_r}{T_r^2},\ B_L = \frac{bP_L}{RT} = 0.0778\frac{P_r}{T_r}(1-\chi) \tag{S10a}$$

$$A_V = \frac{a\alpha(T)P_V}{(RT)^2} = 0.45724\alpha(T)\frac{P_r}{T_r^2},\ B_V = \frac{bP_V}{RT} = 0.0778\frac{P_r}{T_r}(1-\chi) \tag{S10b}$$

$$T_r = \frac{T}{T_c},\ P_r = \frac{P}{P_c} \tag{S10c}$$

where Z_L and Z_V are the compressibility factors of liquid and vapor phases, respectively, P_L is the liquid pressure, P_V is the vapor pressure. The van der Waals mixing rule is then applied to calculate the parameters a and b.

$$a = \sum_i\sum_j x_i x_j a_{ij} = \sum_i\sum_j x_i x_j (1-k_{ij})\sqrt{a_i a_j} \tag{S11a}$$

$$b = \sum_i x_i b_i \tag{S11b}$$

where a_{ij} is the binary interaction of component i and j, k_{ij} is the corresponding binary interaction coefficient of component i and j.

The fugacity coefficient is calculated using the following equations derived from the modified PR-EOS:

$$\ln \varphi_{L}^{i} = -\ln[Z_L - B_L] + \frac{b_i}{b}(Z_V - 1) + \frac{A_L}{2\sqrt{2}B_L}[\frac{1}{a}(2\sum_{j=1}^{N_c} x_j \sqrt{a_i a_j}) - \frac{b_i}{b}]\ln[\frac{Z_L + B_L(1+\sqrt{2})}{Z_L + B_L(1-\sqrt{2})}] \quad (S12a)$$

$$\ln \varphi_{V}^{i} = -\ln[Z_V - B_V] + \frac{b_i}{b}(Z_V - 1) + \frac{A_V}{2\sqrt{2}B_V}[\frac{1}{a}(2\sum_{j=1}^{N_c} x_j \sqrt{a_i a_j}) - \frac{b_i}{b}]\ln[\frac{Z_V + B_V(1+\sqrt{2})}{Z_V + B_V(1-\sqrt{2})}] \quad (S12b)$$

where φ_{L}^{i} and φ_{V}^{i} are the fugacity coefficients of component *i* in liquid and vapor phases, respectively, N_c is the component number of mixtures.

The vanishing IFT method to determine MMP is applied.[S4] The workflow of the proposed method is shown in Fig. S8.

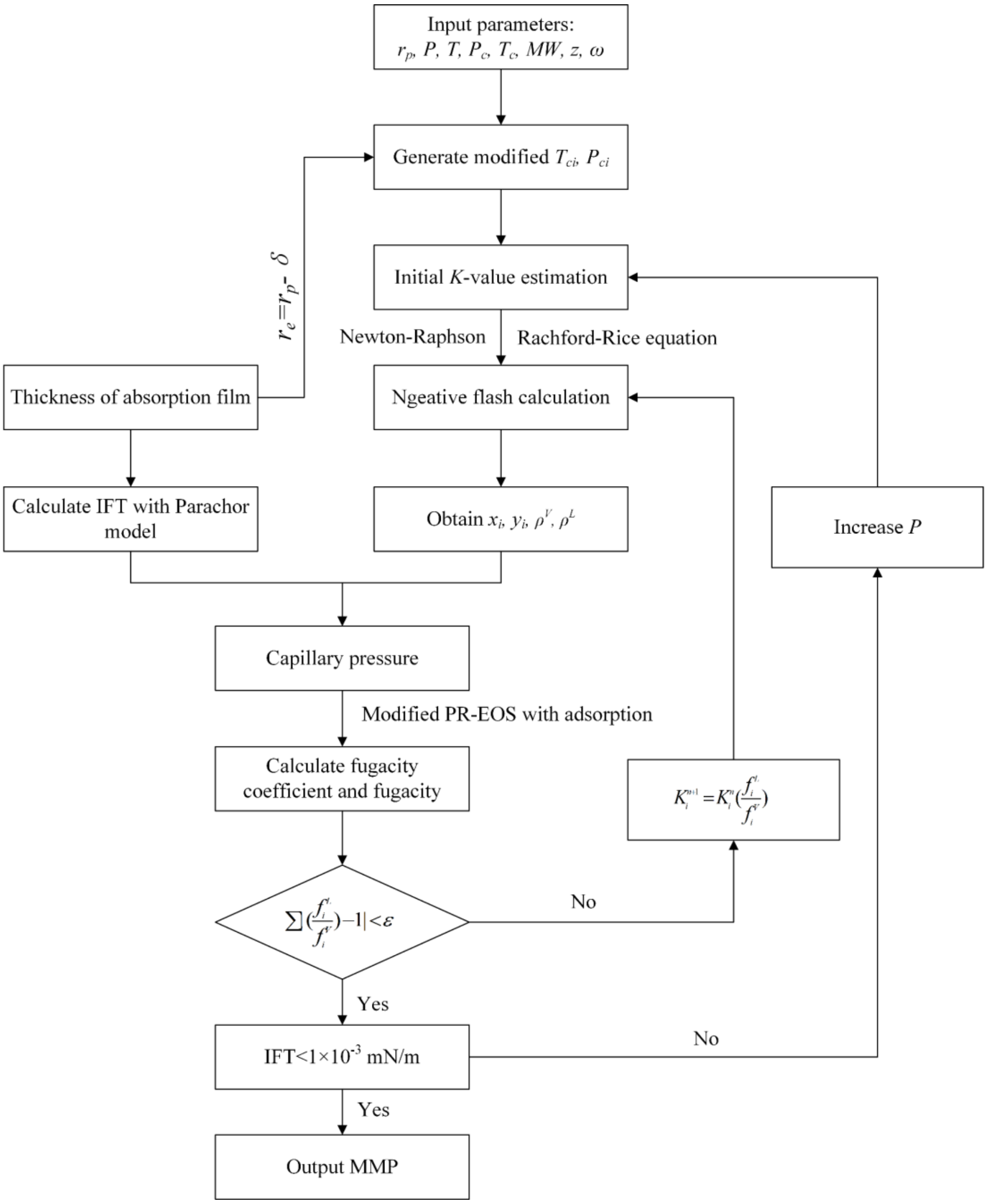

Fig. S8 Flowchart of nanoscale CO_2-hydrocarbon MMP calculation.

Fig. S9 showed the method for calculating the MMP of CO_2 and heptane at 100 nm and 65 °C. The interfacial tension decreases with the increase of system pressure. At 10.4 MPa, the interfacial tension between CO_2 and heptane decreases to 0, thus the CO_2-heptane MMP at 100 nm and 65 °C is 10.4 MPa.

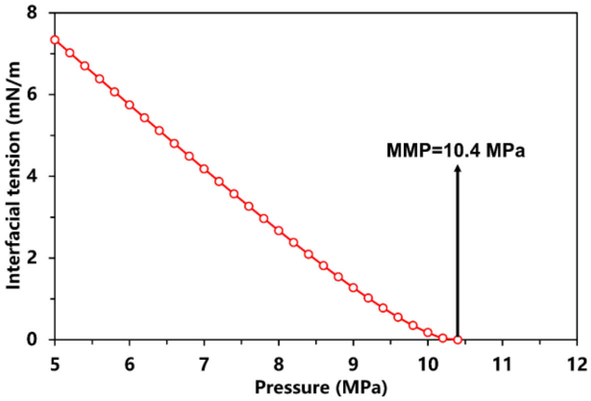

Fig. S9 Interfacial tension between CO_2 and heptane at various pressure and 65 °C.

Section 7: Effects of temperature on MMP

We extended our theoretical model to predict CO_2-heptane MMP at various temperatures and 100 nm (Fig. S10). The model showed that MMP first increases with rising temperature, reaching a peak of 13.8 MPa at 150 °C. Beyond 150 °C, the hydrocarbon mixture behaves more like a vapor, and the reduced density difference between the vapor and liquid phases leads to a decrease in interfacial tension, ultimately causing the MMP reduction.[S5]

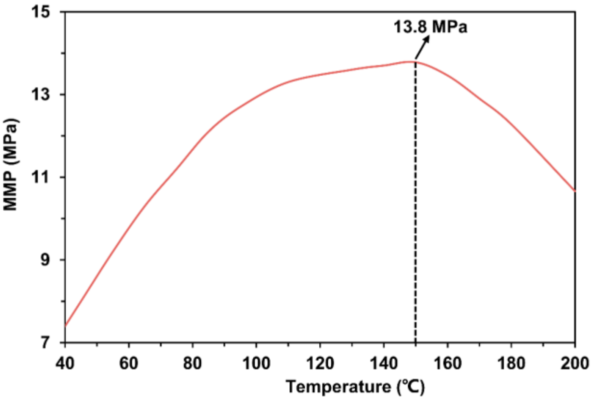

Fig. S10 Calculated CO_2-heptane MMP at 100 nm and various temperatures.

Section 8: Effects of confinement on MMP

We calculated the CO_2-pentane/dodecane MMP across different pore radii using the verified theoretical method. We observed that nanoscale MMP begins to deviate from bulk values when pore radius falls below 500 nm, with this reduction becoming more pronounced as the pore radius decreases (Fig S11a). The reduction of MMP can be attributed to the combined effects of molecular adsorption, capillarity, and critical point shift. Molecular adsorption reduces the amount of free molecules and the effective pore radius (Fig S11b), leading to a larger density difference between vapor and liquid compared with bulk values.[S6] Capillarity induces an additional pressure difference (i.e., capillary force) due to the curvature of the fluid interface within nanopores, resulting in a higher pressure in the gas phase relative to the liquid phase (Fig. S11c). This pressure difference encourages lighter components to condense from vapor to liquid phase, thereby reducing the density difference between two phases.[S7] Critical point shift changes the critical temperature and pressure of confined fluid, altering its phase equilibrium.[S8] This change reduces the differences in composition between the liquid and vapor phases, making them more similar in behavior.[S9] Under the combined effects of molecular adsorption, capillarity, and critical point shift, the density difference between gas and liquid phases is reduced (Fig S11d), leading to a decrease in IFT (Fig. 11c) and a subsequent reduction in MMP.

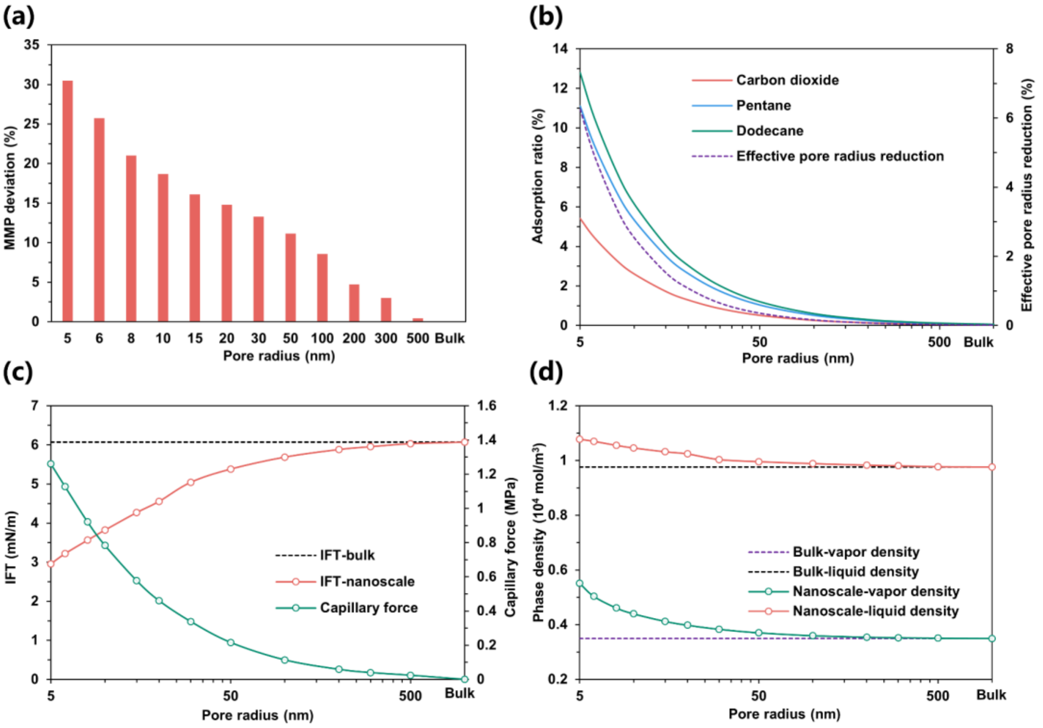

Fig. S11 Effect of nano-confinement on CO_2-pentane/dodecane MMP at various pore radii and 45 °C. (a) Deviation of nanoscale CO_2-pentane/dodecane MMP from bulk value at various pore radii. (b)

Adsorption ratio of various molecules and effective pore radius reduction at different pore radii. (c) Changes in IFT and capillary force with varying pore radii at 6 MPa and 45 °C. (d) Phase density variation across different pore radii at 6 MPa and 45 °C.

To further understand the individual impacts of nano-confinement effects on the confined MMP, we calculated the CO_2-pentane/dodecane MMP by considering different nano-confinement effects (e.g., adsorption, capillarity, and critical point shifts) across various pore radii at 45 °C (Fig. S12a). When pore radius falls below 500 nm, the nanoscale MMP is lower than bulk values, with the reduction becoming more significant as the pore radius decreases. For instance, when considering adsorption, the nanoscale MMP drops from 9.28 MPa to 7.04 MPa as the pore radius decreases from 500 nm to 5 nm. The MMP deviation (compared with the bulk value of 9.32 MPa) increases from 0.43% to 24.46%.

The reduction in nanoscale MMP can be attributed to several mechanisms introduced by nano-confinement. However, the magnitude of this reduction varies depending on the specific nano-confinement effects (Fig. S12b). Among these effects, adsorption leads to the most significant deviation, followed by critical point shifts, with capillarity having the smallest impact. For example, when considering adsorption, the nanoscale MMP at 5 nm drops to 7.04 MPa, a reduction of 24.46% compared with the bulk value of 9.32 MPa. Adsorption's impact on MMP deviation is observed primarily below 500 nm. In contrast, the impact of capillarity results in a smaller reduction, where the MMP decreases to 8.74 MPa, a 6.22% deviation from the bulk value. Capillary effects predominantly affect pores smaller than 30 nm, where capillary pressure becomes significant, but the influence diminishes as pore size increases beyond this threshold. Capillary effects predominantly affect pores smaller than 30 nm, where capillary pressure becomes significant, but the influence diminishes as pore size increases beyond this threshold. Critical point shift leads to an intermediate reduction, with MMP decreasing to 8.32 MPa, corresponding to a 10.73% deviation. The influence of critical point shifts is noticeable below 300 nm.

Adsorption plays a crucial role in influencing the behavior of fluid molecules within nanopores. As pore radii decrease, the enhanced adsorption of fluid molecules on pore walls significantly reduces the quantity of free molecules and effectively narrows the pore radius. As a result of both adsorption effects, the vapor and liquid densities after considering adsorption are higher than bulk values[S1], and the density difference between liquid and vapor becomes larger as well (Fig. S12c). Molecular adsorption also leads to an increase in IFT due to the larger density difference between the liquid and vapor phases.[S10] However, the rate of IFT reduction increases significantly after considering adsorption, resulting in a lower MMP. In contrast, capillarity plays a less prominent role. Within nanopores, the curvature of the fluid interface creates an additional pressure difference (capillary force), resulting in a higher pressure in the gas phase compared with the liquid phase. This pressure differential promotes lighter components to condense from the vapor to the liquid phase[S7], thus reducing the density difference between the two phases and leading to a reduction in IFT and MMP. Notably, the shift in MMP due to capillary effects is only significant when the pore size is below 30 nm, as capillary forces become prominent at this scale. Lastly, shifts in the critical point, while not as significant as adsorption, still impact the MMP by altering the fluid's critical properties under confinement.[S6,S9] This shift leads to a lower MMP, as the confined fluid behaves differently from its bulk counterpart, with critical temperature and pressure deviations contributing to the altered MMP values. This change in phase behavior contributes to an intermediate reduction in MMP.

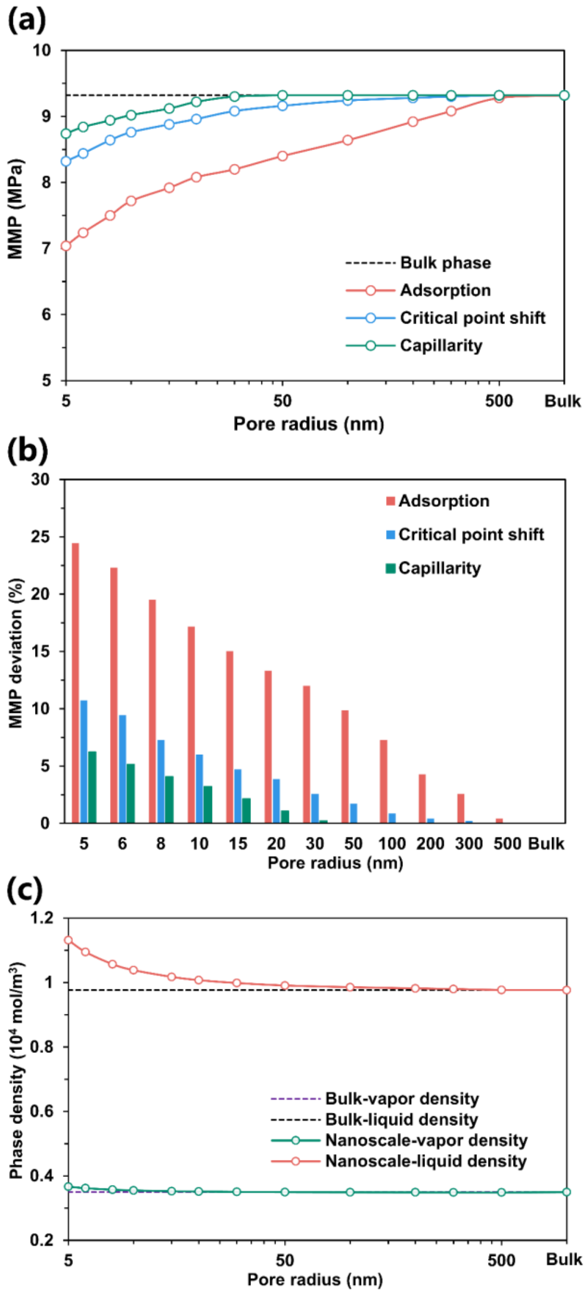

Fig. S12 Effect of different confinements on CO_2-pentane/dodecane MMP at various pore radii and 45 °C. (a) Calculated CO_2-pentane/dodecane MMP with considering different nano-confinement effects at various pore radii and 45 °C. (b) Contribution of nano-confinement effects to CO_2-pentane/dodecane MMP deviation at different pore radii and 45 °C. (c) Phase density of CO_2-pentane/dodecane system with different pore radii and 45 °C and 6 MPa.

References:

S1 Z. Wang, T. Liu, S. Liu, C. Jia, J. Yao, H. Sun, Y. Yang, L. Zhang, M. Delshad, K. Sepehrnoori and J. Zhong, *Energy*, 2024, **288**, 129815.

S2 P. Wang, S. Huang, F. Zhao, J. Shi, B. Wang and Y. Li, *Chem. Eng. J.*, 2022, **433**, 133661.

S3 H. Li, D. Yang and P. Tontiwachwuthikul, *Energy Fuels*, 2012, **26**, 1776-1786.

S4 K. Zhang, N. Jia and S. Li, *RSC Adv.*, 2017, **7**, 54164-54177.

S5 H. Sun and H. Li, *Fuel*, 2021, **286**, 119450.

S6 Y. Song, Z. Song, Z. Chen, L. Zhang, Y. Zhang, D. Feng, Z. Wu and J. Wu, *Energy*, 2024, **289**, 130027.

S7 Y. Song, Z. Song, J. Guo, D. Feng and X. Chang, *Ind. Eng. Chem. Res.*, 2021, **60**, 5300-5309.

S8 K. Zhang, N. Jia and L. Liu, *Chem. Eng. J.*, 2019, **372**, 809-814.

S9 F. Du and B. Nojabaei, *J. Pet. Sci. Eng.*, 2020, **193**, 107362.

S10 S. Wu, Z. Li and H. K. Sarma, *Fuel*, 2020, **262**, 116569.